Environ. Sci. Technol. **2006**, *40,* 462−467

Microscopically Focused Synchrotron X-ray Investigation of Selenium Speciation in Soils Developing on Reclaimed Mine Lands

AMY L. RYSER,† DANIEL G. STRAWN,*,† MATTHEW A. MARCUS,‡ SIRINE FAKRA,‡ JODI L. JOHNSON-MAYNARD,† AND GREGORY MÖLLER†

University of Idaho, Moscow, Idaho, and Lawrence Berkeley National Laboratory, Berkeley, California

Chemical speciation determines Se solubility and therefore its bioavailability and potential for transport in the environment. In this study we investigated the speciation of Se in soil developed on reclaimed mine sites in the U.S. Western Phosphate Resource Area (WPRA) using micro-X-ray absorption near-edge structure (μ-XANES) spectroscopy and micro-X-ray fluorescence (μ-XRF) mapping. Selenium was nonuniformly distributed in the soils and positively correlated with Fe, Mn, Cu, Zn, and Ni. Sixteen points of interest (POI) from three soil samples were analyzed with μ-XANES spectroscopy. The XANES data indicated that Se is present in the soils in at least three oxidation states, Se(−II, 0), Se(IV), and Se(VI). Selenides or elemental Se dominated 7 of the 16 POI. Selenate was the dominant species at only one of the POI. The remaining eight POI were composed of both Se(IV) and Se(VI), with minor Se(−II, 0) contributions. The results of this research suggest that the reduced Se species in the soil parent material are oxidizing to Se(VI), one of the more mobile species of Se in the environment. This information can be used to better predict and manage Se availability in soils.

Introduction

Selenium enrichment is common in sedimentary rocks, and consequently, extraction of coal, oil, and sedimentary ore has displaced Se-bearing rocks into more rapid weathering environments, resulting in increased Se levels in associated ecosystems. One example of this is in the Western Phosphate Resource Area (WPRA), located in southeast Idaho, northern Utah, and western Wyoming. During phosphate ore removal, rock that was not economically valuable was redeposited on the surface as mine backfill. One of the mining byproducts, known as middle waste shale, contains elevated levels of reduced Se species (Se(−II) and Se(0)) (*1*, *2*). As the middle waste shale weathers, reduced Se phases are oxidized to Se-(IV) and Se(VI) species, which are more soluble, bioavailable, and mobile than reduced forms.

Selenium is an essential micronutrient for humans and animals. Generally, diets containing 0.1−0.3 mg kg^{-1} Se are adequate for various animals, while diets that are in excess of 3−15 mg kg^{-1} can cause toxicity (*3*). Mortality of livestock due to selenosis poisoning has been linked to elevated Se levels in water and vegetation in the WPRA (*4*).

The uptake of Se by plant roots depends on soil oxidation state, pH, chemical and mineralogical composition, and the concentration of Se and competing anions such as sulfate and phosphate in solution (*5*−*7*). A general characteristic of Se that can be used to predict bioavailability is oxidation state. Elemental Se(0) and metal selenides, such as Se(−II), have low solubility and therefore low bioavailability and mobility (*8*). Selenite (SeO_3^{2-}) and selenate (SeO_4^{2-}) are the most soluble species (*9*). Selenite is thermodynamically favored under mildly oxidizing conditions (*10*) and has a strong affinity for sorption by Fe oxides such as goethite, amorphous Fe hydroxides, and Al hydroxides (*9*, *11*). Selenate is the most soluble Se species and can be taken up by plants and leached through the soil profile (*10*). Distribution of selenite and selenate between the solid and solution phases within soil is a function of pH and mineral species present.

Since plants growing on the WPRA reclaimed mine soils contain elevated concentrations of Se (*12*), and selenate is the most soluble Se species, it is expected that selenate is present in the soils. Previous studies (*13*) observed that selenate was the only detectable species in water from vadose zone samples in reclaimed soils and in seeps and streams directly impacted by waste rock impoundments. Bond (*14*) conducted leaching and sequential extraction experiments on unweathered waste rock fractions from the WPRA and found that selenite was the primary leachable species and that reduced Se compounds made up the remaining soil Se. Hence, the mobilization of Se from these soils includes species transformations arising from both abiotic and biotic weathering processes.

Sequential extraction is one of the most widely used methods to speciate Se in soil (*15*−*17*). Sequential extractions, however, are operationally defined and results may be inaccurate (*18*). X-ray absorption spectroscopy (XAS) can detect Se species in the soil without any pretreatment or extractions (*19*) and has been used to identify solid-phase Se species in sediments (*2*, *20*−*22*) and plant material (*23*, *24*). Pickering et al. (*20*) used X-ray absorption fine structure (XAFS) spectroscopic techniques to determine that the major Se phases present in evaporation ponds in Kesterson Reservoir, CA were monoclinic elemental Se (red Se) and some aqueous selenite. Micro-XAS (μ-XAS) techniques allow for additional insights into the micromorphology and chemical speciation of heterogeneous soil samples, allowing for increased information on Se biogeochemical cycling in soils (*21*, *22*, *25*, *26*).

To date, most of the research on Se speciation in the WPRA has focused on the Se species present in the middle waste shale (*1*, *2*, *27*). Investigations of reclaimed soils in which weathering and soil development have occurred will allow for a better understanding of the cycling and fate of Se throughout the WPRA. These data can then be used to develop more comprehensive reclamation and management plans that reduce exposure risks.

Materials and Methods

Soil Sample Collection. Soil samples were collected from the Conda mine in the Caribou National Forest, ID. Three soil samples were collected from two plots within a 13 m by 40 m research site. The site was reclaimed 20 years ago, when it was seeded with brome grass (*Bromus marginatus*) and

* Corresponding author phone: (208)885-2713; fax: (208)885-7760; e-mail: dgstrawn@uidaho.edu.
† University of Idaho.
‡ Lawrence Berkeley National Laboratory.

10.1021/es051674i CCC: $33.50

Published on Web 12/13/2005

alfalfa (*Medicago sativa*) as primary species. There were no observable differences between plots in vegetation density or surface features. Soil samples 1 and 3 (S1, S3) came from a depth of 0−20 cm, while soil sample 2 (S2) was taken from the 21−40 cm section at the same location as S1. Soil aggregates (generally less than 1 mm) from the samples were dispersed between either Mylar X-ray film (S2 and S3) or Kapton tape (S1).

The soils were sampled in October of 2003 under dry conditions, and were allowed to further air dry in the laboratory. Martens and Suarez (*28*) showed that air-drying soil samples did not substantially alter the Se speciation in soils from oxidizing environments. Thus, the Se speciation measured in this study by XAS analysis represents in situ conditions.

The clay size fraction was isolated and used to quantify the amount and types of iron oxides present using selective dissolution techniques (*29*). Total organic carbon was measured on a soil sample leached with $FeCl_2$ and 2 M HCl on a CNS analyzer (Elementar Americas, Hanau, Germany) (*30*). Total Se was measured by digestion in nitric, sulfuric, and perchloric acids and analysis of the HCl-reduced digest by hydride generation ICP.

X-ray Spectroscopy. Micro-XANES and fluorescence microprobe mapping were done on beamline 10.3.2 at the Advanced Light Source (ALS), Lawrence Berkeley National Laboratory (Berkeley, California) (*31*). Samples were attached to an *XYZ* stage oriented 45° to the beam, using double-sided tape. For elemental mapping microsynchrotron X-ray fluorescence (μ-SXRF) was used. The elemental distribution maps were collected using a beam focused to 7 μm by 7 μm (H × V) or 11μm by 7 μm using a 7−10 μm pixel size. Dwell time per point was 100 ms. The beam energy was tuned to 12757 eV. The windowed (regions of interest) X-ray fluorescence counts for As, Ca, Cr, Cu, Fe, Mn, Ni, Se, Ti, and Zn were raster-scanned through the beam.

A Se oxidation state map was collected for sample S2. The sample was mapped at two fixed incident photon energies such that the ratio of the X-ray absorption between these energies was most sensitive to the oxidation state of the Se, owing to the chemical shift of the absorption edge. The two energies correspond to maximum energies for Se(0)/Se(IV) (12658.8 eV) and Se(IV)/Se(0) (12664.5 eV). The beam was focused to 5 μm by 5 μm, and the step size was 3 μm. The fluorescence data are presented as bicolor maps that allow qualitative analysis of the oxidation state distribution when the background signal is small compared to that of the Se K-edge fluorescence.

Selenium salt standards were purchased from Alfa Aesar or Sigma Aldrich, and select minerals were purchased from the Excalibur Mineral Company (New York). Ferroselite was synthesized following the procedures described by Warren (*32*), and its structure confirmed using powder X-ray diffraction. Monoclinic elemental Se was made by microbial reduction of selenite. Standards were diluted in boron nitride. Standards for selenite and selenate sorbed onto goethite were prepared by sorbing either 0.01 mM sodium selenite (Na_2SeO_3) or sodium selenate (Na_2SeO_4) onto goethite at pH 4.5. Selenite- and selenate-spiked ferrihydrite and calcite were prepared in the same manner, except at pH 7.0.

All XANES spectra were collected at room temperature. Selected Se standards were measured on beamline 10.3.2. Additional Se standards were measured on beamline X-11b at the National Synchrotron Light Source (NSLS) at Brookhaven National Laboratory, Upton, New York. Transmission spectra from Se standards diluted in boron nitride were collected using an ionization detector. Orthorhombic elemental Se was run either between samples (beamline 10.3.2) or in situ (X-11b) to correct for beam energy shifts. Scans of elemental Se at both beamlines showed that the XANES features were comparable between the two beamlines.

The XAS data were merged (3−7 scans), normalized, and background subtracted using standard procedures in the program ATHENA (*33*). Step size through the XANES regions was 0.70 eV. Measurement of the standard deviation of the edge energies from several points of interest (POI) with the same XANES features between two separate beamtime runs indicated that the edge energy precision was less than the step size. Thus, we estimate that the calibrated data were accurate to within 0.70 eV.

To provide quantitative information about the different forms of Se linear least-squares combination fitting of the XANES data was done using ATHENA (*33*). The experimental spectra were fit with various linear combinations of Se standards, and the best fit represents the composition of the experimental spectra. The data were fit in the energy range ±20 eV from the Se(0) edge. Accuracy and sensitivity were evaluated by comparing fit results to theoretical mixtures.

To test the effects of possible radiation-induced reduction (RIR) on soil samples we collected several successive scans of sodium selenite and sodium selenate sorbed onto goethite. Goethite-sorbed selenite and selenate were placed on a sample holder and either held in place by Kapton tape or Mylar film. From six to eight successive scans of the samples were collected, with each scan taking 5 min. RIR of selenate but not selenite was observed on the goethite (Supporting Information Figure S1). To monitor possible RIR of Se in the soil samples, successive 5 min XANES scans were collected on each point prior to longer scans needed for full XANES data processing and analysis. RIR was not observed in any of the successive scans of the soil samples.

Results and Discussion

Sensitivity of Se XANES Spectra. The absorption edge energies (first inflection point) for Se(IV) and Se(VI) compounds are 12662.0 and 12664.0 eV, respectively. Reduced Se compounds have variable edge energies between 12657.5 and 12659.5 eV (Supporting Information Figure S2), depending on structural arrangement and the type of atoms in the compound or mineral. Both allotropes of zero-valent Se have edge energies of 12658.0 eV. For selenides the edge energies range between 12656.0 and 12658.0 eV. Edge energies for organic Se compounds range from 12657.5 to 12659.5 eV.

Linear combination fitting of all samples was done using elemental Se (orthorhombic) and selenite and selenate sorbed to goethite. Fitting lacked sensitivity for reduced Se compounds (Se(−II, 0)) when selenite and selenate species were present in the sample. As an example, sample S2 POI a was fit using Se-cystine (Figure 1), selenite on goethite, and selenate on goethite, resulting in 22% Se-cystine, 62% Se(IV), and 16% Se(VI). When Se-cystine was replaced with elemental Se, the fit combination changed to 20% elemental Se, 64% Se(IV), and 16% Se(VI), with an insignificant difference in the residual error. There are several possible reasons for this lack of sensitivity: (1) there is little difference between the reference spectra (e.g., Se-spiked goethite and Se-spiked ferrihydrite XANES are indistinguishable (Supporting Information Figure S2)); (2) some of the spectral features of the reduced Se compounds are not unique; (3) heterogeneity in overabsorption (*34*); and/or (4) lack of appropriate standards. Pickering et al. (*24*) modeled Se in milk vetch (*Astragalus bisulcatus*) using linear combinations of selenate and selenomethionine. In their results fitting was robust because of the limited number of possible species present and the absence of the intermediate Se(IV) in the spectra.

The soil samples used in this study contain Se(−II, 0), Se(IV), and Se(VI) species resulting in overlapping white lines and edges. Additionally, there are several types of Se species

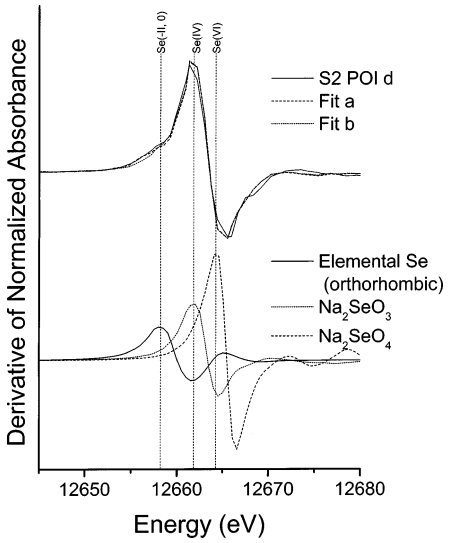

FIGURE 1. Linear combination fitting results for the S2 POI d fit with Se-cystine, selenite, and selenate (fit a) and elemental Se, selenite, and selenate (fit b) compared to standards.

that could be present in the soils. For these reasons, and because linear combination fitting has limited sensitivity for Se XANES, the accuracy of fitting complex unknown mixtures such as soils is poor. Ostergren et al. (*35*) suggested that the error in the linear combination (LC) fit results from extended X-ray adsorption fine structure (EXAFS) fit data may be as high as 25%, and the presence of species with LC contributions less than 10% is questionable. Despite lack of sensitivity and accuracy in LC fitting for specific Se compounds or mineral species, determining the presence of the oxidation state based on linear combinations of the compound classes Se(−II, 0), Se(IV), and Se(VI) was robust. Thus we have interpreted the XANES spectrum from samples analyzed in this research on a semiquantitative scale. If the LC fit resulted in a particular oxidation state class which was greater than 45% of the XANES spectrum then it was classified as the dominant contribution to the XANES spectrum, less than 45% but more than 25% was classified as medium, and less than 25% but more than 10% was classified as a minor component of the XANES spectrum. If the oxidation state class contribution was less than 10% it was considered negligible.

Soil Properties. The soils sampled in this study have silt loam textures (14% sand, 61% silt, and 25% clay) for both the surface and subsurface horizons. Iron in soils is an important mineral for adsorption of Se, thus controlling its fate in the environment. The average total Fe in the samples was 4.2% (by mass) with 27% Fe as goethite, 11% as poorly crystalline Fe (i.e., ferrihydrite), 3% bound to organic matter, and 59% residual Fe in primary mineral form. The average amount of organic carbon in the soils was 4.3%, and the average pH of the soil was 7.7. Concentrations of Fe and organic carbon and pH values are similar to results obtained by Bond (*14*) from reclaimed soils at the nearby Smokey Canyon mine site, southwestern Idaho. Total Se concentrations were 14, 70, and 26 mg kg^{-1} for samples S1, S2, and S3, respectively.

Elemental Distribution in the Soil. Microspectroscopic analyses include collecting a μ-SXRF elemental map of a selected region in a sample, selecting POI from the elemental map, and collecting XANES data on each POI. A μ-SXRF bicolor elemental distribution map for Fe and Se in S3 is shown in Figure 2 (Fe and Se distribution maps for samples S1 and S2 are shown in Supporting Information Figure S3). Selenium was plotted with Fe because these elements are commonly observed together in soils and the middle waste shale parent material (*1*, *2*). The Se distribution clearly shows

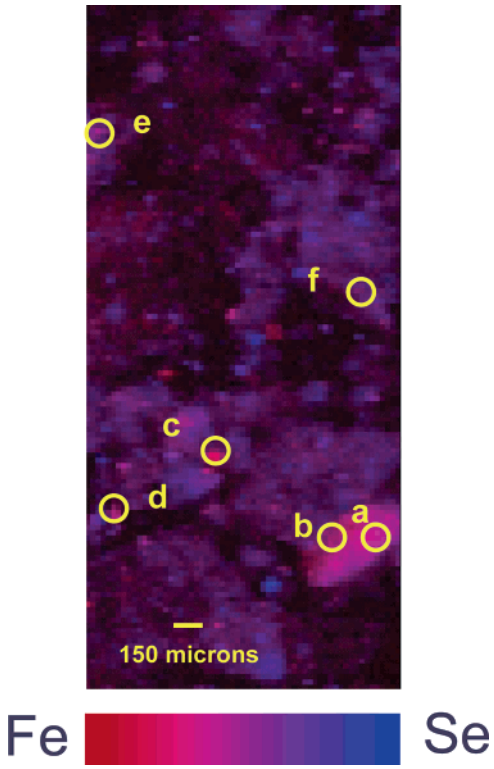

FIGURE 2. Bicolor μ-SXRF map of the reclaimed mine soil sample S3. The letters next to the circles indicate points of interest (POI). The color bar indicates the degree of codistribution of the two elements. Where the elements are not colocated the color is either pure red (Fe) or pure blue (Se); when the elements are both located at a pixel spot red and blue are mixed resulting in the colors indicated in the color mixing bar.

TABLE 1. Pearson's Correlation Coefficients between Selenium and Other Elements for Soil Samples S1, S2, and S3[a]

element	S1 (n = 13680)	S2 (n = 11900)	S3 (n = 10298)
As		0.484	0.708
Ca	0.337	0.025	0.440
Cr	0.670	0.270	0.657
Cu	0.965	0.329	0.779
$FeK_{\alpha 1}/MnK_{\beta 1}$	0.429	0.566	0.630
Mn	0.667	0.510	0.614
Ni	0.808	0.429	0.717
Ti	0.294	0.086	0.427
Zn	0.939	0.442	0.777

[a] Significant correlation at P = 0.05.

preferential partitioning of Se in the soils, indicating that Se mineral concentrations exceed bulk soil Se concentrations. Such information on Se partitioning is critical for evaluating Se reactivity.

The elemental distribution maps showed that the soils contained hotspots of Fe, As, Ca, Cr, Cu, and Zn. XRF from two spots (data not shown) also showed that S and V were present. The elements identified in the reclaimed soil have been observed in the parent material (middle waste shale) (*36*) and also in the reclaimed mine soils (*14*). To assess whether there were significant correlations between Se and elements of interest, paired elemental concentrations (intensity) from the μ-SXRF xy-scan of the samples were plotted against each other. Table 1 shows Pearson's correlation coefficients between Se and As, Ca, Cr, Cu, Fe, Mn, Ni, Ti, and Zn. There were significant correlations between Se and Fe, Mn, Cu, Zn, and Ni (although S2 correlations were lower

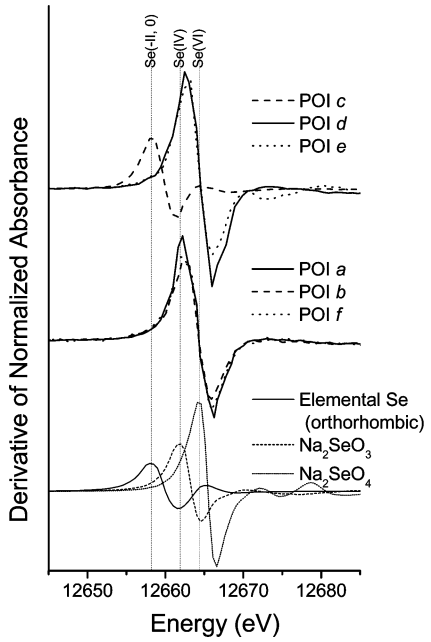

FIGURE 3. Selenium micro-XANES spectra for sample S3. The figure contains the spectra for all points of interest (POI) and standards.

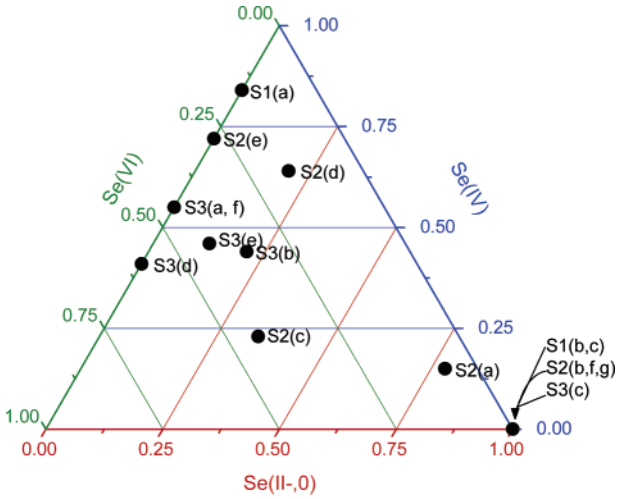

FIGURE 4. Ternary diagram showing LC fit results using elemental selenium and selenite and selenate adsorbed on goethite for all POI from samples S1, S2, and S3. The labels to the right of the dots correspond to the POI labeled in Figure 3 and Figure S3 in the Supporting Information.

than those for S1 and S3). There was a low (nonsignificant) correlation between Se and Ca for all soil samples, which was also observed in the middle waste shale (*1*), suggesting that Se does not associate with calcite minerals in the soils. Perkins and Foster (*2*) observed that a Cu−V mineral (sulvanite) in middle waste shale rock had the highest Se concentrations. The highest correlation in the soils was between Se and Cu; in addition, the XRF spectra showed high concentrations of V at some POI, supporting the findings of Perkins and Foster (*2*).

XANES Oxidation State Determination. The selenium oxidation state was determined by comparing the XANES derivative spectra (Figure 3 shows the spectra for S3; spectra for S1 and S2 are shown in Supporting Information Figure S4). Results from the linear combination fits of the Se XANES spectra from the three soil samples are shown in Figure 4. Six of the sixteen POI collected across the three samples contained only Se(−II, 0) species. Selenite was the dominant fit component in six of the POI XANES. The Se(VI) standard was a dominant fit component in three POI XANES spectra and only predominated in one spectrum, S3 POI d.

The presence of Se(−II, 0) was expected since metal and organic selenides exist in the middle waste shale parent material (*1*). Selenite has been observed in weathered shales (*2*); however, Ryser et al. (*1*) did not find Se(IV) in unweathered shale. Thus, we hypothesize that the Se(IV) observed in the soil occurs from weathering and oxidation of the metal selenides. Although near-neutral pH and oxic conditions suggest that Se(VI) is thermodynamically stable (*37*), its presence in WPRA reclaimed soils has not been confirmed. In addition to being found in plants growing on the reclaimed soils (*12*), elevated Se levels have also been found in water, sediments, soil leachate, aquatic plants, invertebrates, and fish in streams near the phosphate mining areas (*38*). The presence of Se throughout the ecosystem indicates that Se is mobile in the WPRA. Jayaweera and Bigger (*39*) observed that when reduced rice paddy soils were subject to oxidizing conditions the total soluble Se and Se(VI) continually increased, while Se(IV) increased initially, but eventually decreased (*39*). In the reclaimed WPRA soils the oxidizing environment is such that the Se(VI) species is favored. However, its minimal presence compared to that of Se(IV) suggests that Se(VI) is quickly leached from the soils, accounting for the presence of Se throughout the ecosystem.

Several POI were composed of multiple Se oxidation states. To better resolve the oxidation state distribution, the region surrounding S2 POI a was mapped at two different energies sensitive to reduced and oxidized Se species: Se(−II, 0) and Se(IV) (Figure 5A). Contributions from Se(VI) may be present in the Se(IV) energy scan. Total relative Se and Fe spatial distributions are also shown (Figure 5B). The advantage of energy specific mapping, as opposed to scanning the XANES energy region from a single spot, is that relative distribution information on oxidation states can be obtained, allowing for comparison of oxidation state distribution. From the bicolor map it appears that there is a reduced (Se(−II, 0) grain approximately 15 μm in diameter sitting on top of an approximately 100 μm diameter iron oxide aggregate with selenite adsorbed (Figure 5). The scatter plot of the Se(IV) versus Se(−II, 0) intensities (Supporting Information Figure 5) shows a distinct decrease in the relationship at the higher Se counts, indicating there are two populations of data; one with more Se(IV) than Se(0), and visa versa, thereby confirming the presence of two different mineral particles. Oxidation state mapping has been successfully applied to analyze the oxidation state of Se in plants (*24*). Sutton et al. (*40*) mapped Se oxidation states in a flooded soil−root system spiked with Se(VI) and observed that Se(0) and Se(IV) had distinct distributions that corresponded to microbial activity. Although we were only able to map one region, the spatial distribution of the species gained from this research clearly shows the potential for interpreting processes such as mineral weathering and formation in natural heterogeneous environments, such as soils.

Three Se oxidation states were identified from micro-XANES data. Results from sequential extractions and leaching experiments on reclaimed mine soils in the WPRA indicated that extractable Se in the unweathered waste rock fractions primarily exists as selenite, with the remaining species present in the soil as either selenides or elemental Se (*14*). The micro-XANES from this study indicated that Se(VI) was present, although it does not appear to be as prevalent as Se(IV). Neal and Sposito (*41*) showed that selenate adsorption in four soils was insignificant between pH 5.5 and 9. Thus, based on the 7.7 pH of the reclaimed soils, we expect very little selenate retention, i.e., when Se(IV) is oxidized to Se(VI) it will be either taken up by plants or leached out of the profile.

Below pH 7 selenite will be primarily sorbed to iron oxide surfaces, while above pH 8 selenite adsorption is minimal

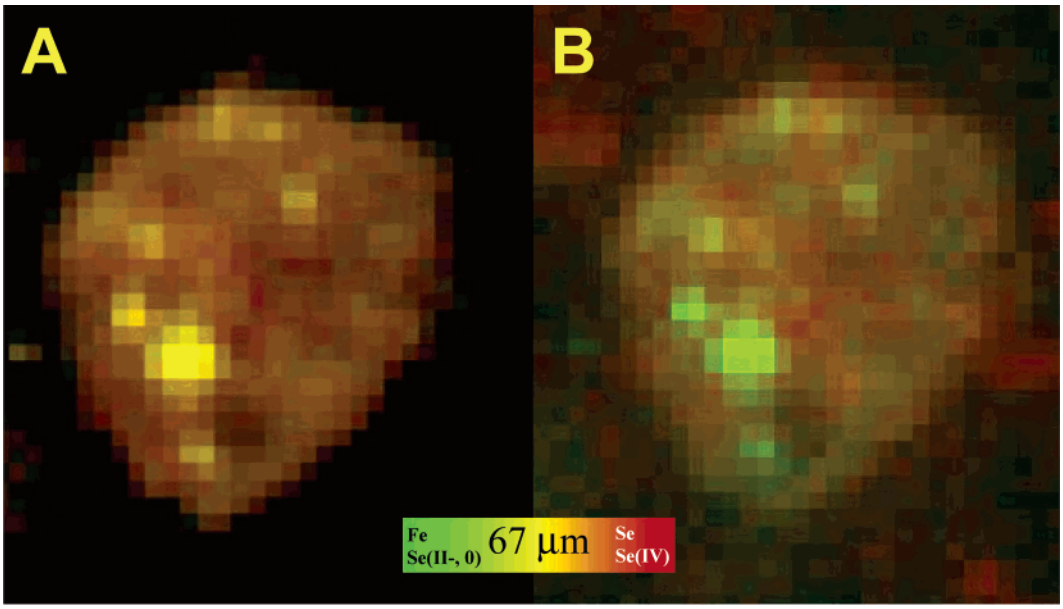

FIGURE 5. Bicolor micrographs for Se oxidation states (panel A) and Se and Fe distribution (panel B). The color bar indicates relative mixing of oxidation states and Fe and Se. Micrograph A is an oxidation state map created by mapping at 12658.8 eV where the Se(0)/Se(IV) was maximized (green), followed by another scan at 12664.5 eV where Se(IV)/Se(0) was maximized (red). The resulting micrograph indicates the relative spatial distributions of Se(−II, 0) and Se(IV). Micrograph B is a bicolor map for total Se (green) and iron (red) scanned at 12683.0 eV. Brightness, saturation, and contrast were modified to enhance spatial distribution information.

(*11*). The neutral to alkaline pH of the soils suggest that selenite may be available for leaching or plant uptake. Selenite adsorption on iron oxides is also dependent on the presence of other anions. If strongly bound anions such as phosphate or organic acids are present in high concentrations compared to that of selenite, then competition would cause Se to partition into the aqueous phase, thus making selenite mobile in the environment (*42*). Bond (*14*) reported that reclaimed soils in the WPRA contained plant-available phosphorus at slightly higher than normal concentrations, suggesting that selenite would have to compete with phosphate for adsorption sites in these soils. Competition with phosphate for adsorption sites could potentially increase selenite bioavailability.

The presence of reduced Se species together with selenite in the reclaimed mine soils suggests that primary Se-bearing minerals still exist. Because these soils are relatively young, and the kinetics of oxidation of reduced Se species is slow (*43*, *44*), oxidation and mobilization will continue. Speciation results from this research will improve risk assessment and remediation strategies for the WPRA environment. Additionally, insights gained from the research provide new knowledge that can be applied to understanding biogeochemical cycling of Se in environments where Se-bearing sedimentary rocks are present.

Acknowledgments

Funding for this project was provided by the U.S. Environmental Protection Agency Grant ID No. X970339010. The Advanced Light Source is supported by the Director, Office of Science, Office of Basic Energy Sciences, Materials Sciences Division, of the U.S. Department of Energy under Contract No. DE-AC03-76SF00098 at Lawrence Berkeley National Laboratory. Research carried out (in whole or in part) at the National Synchrotron Light Source, Brookhaven National Laboratory, is supported by the U.S. Department of Energy, Division of Materials Sciences and Division of Chemical Sciences, under Contract No. DE-AC02-98CH10886. Assistance from Brian Hart is appreciated.

Supporting Information Available

Data showing RIR experiments, Figure S1; XANES spectra for standards, Figure S2; μ-SXRF and μ-XANES from samples S1 and S2, Figures S3 and S4; scatter plot of the Se oxidation state map in Figure 5, Figure S5. This material is available free of charge via the Internet at http://pubs.acs.org.

Literature Cited

(1) Ryser, A. L.; Strawn, D. G.; Marcus, M. A.; Johnson-Maynard, J. L.; Gunter, M. E.; Moller, G. Micro-spectroscopic investigation of selenium-bearing minerals from the Western US Phosphate Resource Area. *Geochem. Trans.* **2005**, *6*, 1−11.

(2) Perkins, R. B.; Foster, A. L. Mineral affinities and distribution of selenium and other trace elements in black shale and phosphorite of the Phosphoria formation. In *Life Cycle of the Phosphoria Formation: From Deposition to Post-Mining Environment*; Hein, J. R., Ed.; Elsevier B. V.: Amsterdam, The Netherlands, 2004; Vol. 8, pp 251−295.

(3) Mayland, H. F. Selenium in plant and animal nutrition. In *Selenium in the Environment*; Frankenberger, W. T., Benson, S., Eds.; Marcel Dekker: New York, 1994; pp 29−69.

(4) Piper, D. A.; Skorupa, J. P.; Presser, T. S.; Hardy, M. A.; Hamilton, S. J.; Huebner, M.; Gulbrandsen, R. A. The Phosphoria Formation at the Hot Springs mine in Southeastern Idaho: a source of selenium and other trace elements to surface water, groundwater, vegetation, and biota. *U. S. Geol. Survey Open−File Rep. 00-050* **2000**, 73.

(5) Mikkelsen, R. L.; Page, A. L.; Bingham, F. T. Factors affecting selenium accumulation by agricultural crops. In *Selenium in Agriculture and the Environment*; Jacobs, L. W., Ed.; SSSA: Madison, WI, 1989; Vol. SSSA Special Publication 23, pp 65−94.

(6) Baylock, M. J.; James, B. R. Redox transformation and plant uptake of Se resulting from root−soil interactions. *Plant Soil* **1994**, *158*, 1−17.

(7) Dhillon, K. S.; Dhillon, S. K. Distribution and management of seleniferous soils. *Adv. Agron.* **2003**, *79*, 119−184.

(8) Presser, T. S.; Swain, W. C. Geochemical evidence for Se mobilization by the weathering of pyritic shale, San Joaquin Valley, California, USA. *Appl. Geochem.* **1990**, *5*, 703−717.

(9) McNeal, J. M.; Balistrieri, L. S. Geochemistry and occurrence of selenium: An overview. In *Selenium in Agriculture and the Environment*; Jacobs, L. W., Ed.; ASA and SSSA: Madison, WI, 1989; Vol. SSSA Special Publication Number 23, pp 1−13.

(10) Elrashidi, M. A.; Adriano, D. C.; Workman, S. M.; Lindsay, W. L. Chemical equilibria of selenium in soils: A theoretical development. *Soil Sci.* **1987**, *144*, 141−152.

(11) Balistrieri, L. S.; Choa, T. T. Selenium absorption by goethite. *Soil Sci. Soc. Am. J.* **1987**, *51*, 1145−1151.
(12) Mackowiak, C. L.; Amacher, M. C.; Hall, J. O.; Herring, J. R. Uptake of selenium and other contaminant elements into plants and implications for grazing animals in southeast Idaho. In *Life Cycle of the Phosphoria Formation: From Deposition to Post-Mining Environment*; Hein, J. R., Ed.; Elsevier B. V.: Amsterdam, The Netherlands, 2004; Vol. 8, pp 527−555.
(13) George, J. Chemodynamic Studies of Selenium Release, Mineralization, and Sorption−Desorption Pathways in the Western Phosphate Resource Area. M.S. Thesis, University of Idaho, Moscow, ID, 2002.
(14) Bond, M. M. Characterization and Control of Selenium Releases from Mining in the Idaho Phosphate Region. M.S. Thesis, University of Idaho, Moscow, ID, 1999.
(15) Martens, D. A.; Saurez, D. L. Selenium speciation of marine shales, alluvial soils, and evaporation basin soils of California. *J. Environ. Qual.* **1997**, *26*, 424−432.
(16) Wang, M. C.; Chen, H. M. Forms and distribution of selenium at different depths and among particle size fractions of three Taiwan soils. *Chemosphere* **2003**, *52*, 585−593.
(17) Zawislanski, P. T.; Benson, S. M.; Terberg, R.; Borglin, S. E. Selenium speciation, solubility, and mobility in land-disposed dredged sediments. *Environ. Sci. Technol.* **2003**, *37*, 2415−2420.
(18) Wright, M. T.; Parker, D. R.; Amrhein, C. Critical evaluation of the ability of sequential extraction procedures to quantify discrete forms of selenium in sediments and soils. *Environ. Sci. Technol.* **2003**, *37*, 4709−4716.
(19) Pickering, I. J.; George, G. N.; Fleet-Stalder, V. V.; Chasteen, T. G.; Prince, R. C. X-ray absorption spectroscopy of selenium-containing amino acids. *J. Biol. Inorg. Chem.* **1999**, *4*, 791−794.
(20) Pickering, I. J.; Brown, G. E., Jr..; Tokunaga, T. K. Quantitative speciation of selenium in soils using X-ray absorption spectroscopy. *Environ. Sci. Technol.* **1995**, *29*, 2456−2459.
(21) Tokunaga, T. K.; Sutton, S. R.; Bajt, S. Mapping of selenium concentrations in soil aggregates with synchrotron X-ray fluorescence microprobe. *Soil Sci.* **1994**, *158*, 421−434.
(22) Tokunaga, T. K.; Sutton, S. R.; Bujt, S.; Nuessle, P.; Shea-McCarthy, G. Selenium diffusion and reduction at the water−sediment boundary: Micro-XANES spectroscopy of reactive transport. *Environ. Sci. Technol.* **1998**, *32*, 1092−1098.
(23) Pickering, I. J.; Wright, C.; Bubner, B.; Ellis, D.; Persans, M. W.; Yu, E. Y.; George, G. N.; Prince, R. C.; Salt, D. E. Chemical form and distribution of selenium and sulfur in the selenium hyperaccumulator *Astragalus bisulcatus*. *Plant Physiol.* **2003**, *131*, 1460−1467.
(24) Pickering, I. J.; Prince, R. C.; Salt, D. E.; George, G. N. Quantitative, chemically specific imaging of selenium transformation in plants. *Proc. Natl. Acad. Sci. U.S.A.* **2000**, *97*, 10717−10722.
(25) Strawn, D.; Doner, H.; Zavarin, M.; McHugo, S. Microscale investigation into the geochemistry of arsenic, selenium, and iron in soil developed in pyritic shale materials. *Geoderma* **2002**, *108*, 237−257.
(26) Manceau, A.; Marcus, M. A.; Tamura, N. Quantitative speciation of heavy metals in soils and sediments by synchrotron X-ray Techniques. In *Applications of Synchrotron Radiation in Low-Temperature Geochemistry and Environmental Sciences*; Fenter, P. A., Rivers, M. L., Sturchio, N. C., Sutt, S. R., Eds.; Geochemical Society and Mineralogical Society of America: Washington, DC, 2002; Vol. 49, pp 341−428.
(27) Desborough, G.; DeWitt, E.; Jones, J.; Meier, A.; Meeker, G. Preliminary mineralogical and chemical studies related to the potential mobility of selenium and associated elements in Phosphoria Formation Strata, southeastern Idaho. *U. S. Geol. Survey Open−File Rep. 99−129* **1999**, 20 pp.
(28) Martens, D. A.; Suarez, D. L. Changes in the distribution of selenium oxidation states with sample storage. *J. Environ. Qual.* **1997**, *26*, 1711−1714.
(29) Jackson, M. L.; Lim, C. H.; Zelazny, L. W. Oxides, hydroxides, and alluminosilicates. In *Methods of Soil Analysis Part 1*, 2nd ed.; Klute, A., Ed.; ASA, CSA, and SSSA: Madison, WI, 1986; pp 101−105.
(30) Loeppert, R. H.; Suarez, D. L. Carbonate and Gypsum. In *Methods of Soil Analysis. Part 3*; Spark, D. L., Ed.; Soil Science Society of America and Society of Agronomy: Madison, WI, 1996; pp 437−474.
(31) Marcus, M. A.; MacDowell, A. A.; Celestre, R.; Manceau, A.; Miller, T.; Padmore, H. A.; Sublett, R. E. Beamline 10.3.2 at ALS: a hard X-ray microprobe for environmental and materials science. *J. Synchrotron Radiat.* **2004**, *11*, 239−247.
(32) Warren, C. G. The synthesis of ferroselite from an aqueous solution at low temperature. *Econ. Geol.* **1968**, *63*, 418−419.
(33) Newville, J. IFEFFIT: interactive XAFS analysis and FEFF fitting. *J. Synchrotron Radiat.* **2001**, *8*, 322−324.
(34) O'Day, P. A.; Rivera, N.; Root, R.; Carroll, S. A. X-ray absorption spectroscopic study of Fe reference compounds for the analysis of natural sediments. *Am. Mineral.* **2004**, *89*, 572−585.
(35) Ostergren, J. D.; Brown, G. E.; Tingle, T. N. Quantitative speciation of lead in selected mine tailings from Leadville, CO. *Environ. Sci. Technol.* **1999**, *33*, 1627−1636.
(36) Herring, J. R.; Desborough, G. A.; Wilson, S. A.; Tysdal, R. G.; Grauch, R. I.; Gunter, M. E. Chemical composition of weathered and unweathered strata of the Meade Peak Phosphatic Shale Member of the Permian Phosphoria Formation-A. Measured sections A and B, central part of Rasmussen Ridge, Caribou County, Idaho. *U. S. Geol. Survey Open−File Rep. 99-147-A* **1999**, 24 pp.
(37) Neal, R. H.; Sposito, G.; Holtzclaw, K. M.; Traina, S. J. Selenite adsorption on alluvial soils: I. Soil composition and pH effects. *Soil Sci. Soc. Am. J.* **1987**, *51*, 1161−1165.
(38) Hamilton, S. J.; Buhl, K. J.; Lamothe, P. J. Selenium and other trace elements in water, sediment, aquatic plants, aquatic invertebrates, and fish from streams in SE Idaho near phosphate mining. In *Life Cycle of the Phosphoria Formation: From Deposition to Post-Mining Environment*; Hein, J. R., Ed.; Elsevier B. V.: Amsterdam, Netherlands, 2004; Vol. 8, pp 483−526.
(39) Jayaweera, G. R.; Biggar, J. W. Role of redox potential in chemical transformations of selenium in soils. *Soil Sci. Soc. Am. J.* **1996**, *60*, 1056−1063.
(40) Sutton, S. R.; Bajt, S.; Delaney, J.; Schulze, D.; Tokunaga, T. Synchrotron X-ray fluorescence microprobe: Quanitification and mapping of mixed valence state samples using micro-XANES. *Rev. Sci. Instrum.* **1995**, *66*, 1464−1467.
(41) Neal, R. H.; Sposito, G. Selenate adsorption on Alluvial soils. *Soil Sci. Soc. Am. J.* **1987**, *53*, 70−74.
(42) Dhillon, S. K.; Dhillon, K. S. Selenium adsorption in soils as influenced by different anions. *J. Plant Nutr. Soil Sci.* **2000**, *163*, 577−582.
(43) Dowdle, P. R.; Oremland, R. S. Microbial oxidation of elemental selenium in soil slurries and bacterial cultures. *Environ. Sci. Technol.* **1998**, *32*, 3749−3755.
(44) Losi, M. E.; Frankenberger, W. T. Microbial oxidation and solubilization of precipitated elemental selenium in soil. *J. Environ. Qual.* **1998**, *27*, 836−843.

Received for review August 23, 2005. Revised manuscript received November 1, 2005. Accepted November 3, 2005.

ES051674I